Charge and matter distributions and form factors of light, medium, and heavy neutron-rich nuclei

A. N. Antonov,[1] D. N. Kadrev,[1] M. K. Gaidarov,[1] E. Moya de Guerra,[2] P. Sarriguren,[2] J. M. Udias,[3] V. K. Lukyanov,[4]
E. V. Zemlyanaya,[4] and G. Z. Krumova[5]

[1]*Institute for Nuclear Research and Nuclear Energy, Bulgarian Academy of Sciences, Sofia 1784, Bulgaria*
[2]*Instituto de Estructura de la Materia, CSIC, Serrano 123, E-28006 Madrid, Spain*
[3]*Departamento de Fisica Atomica, Molecular y Nuclear, Facultad de Ciencias Fisicas, Universidad Complutense de Madrid,*
Madrid E-28040, Spain
[4]*Joint Institute for Nuclear Research, Dubna RU-141980, Russia*
[5]*University of Rousse, Rousse 7017, Bulgaria*
(Received 15 June 2005; published 20 October 2005)

Results of charge form factors calculations for several unstable neutron-rich isotopes of light, medium, and heavy nuclei (He, Li, Ni, Kr, Sn) are presented and compared to those of stable isotopes in the same isotopic chain. For the lighter isotopes (He and Li) the proton and neutron densities are obtained within a microscopic large-scale shell-model, while for heavier ones Ni, Kr, and Sn the densities are calculated in deformed self-consistent mean-field Skyrme HF+BCS method. We also compare proton densities to matter densities together with their rms radii and diffuseness parameter values. Whenever possible comparison of form factors, densities and rms radii with available experimental data is also performed. Calculations of form factors are carried out both in plane wave Born approximation (PWBA) and in distorted wave Born approximation (DWBA). These form factors are suggested as predictions for the future experiments on the electron-radioactive beam colliders where the effect of the neutron halo or skin on the proton distributions in exotic nuclei is planned to be studied and thereby the various theoretical models of exotic nuclei will be tested.

I. INTRODUCTION

The scattering of particles and ions from nuclei has provided along the years invaluable information on charge, matter, current, and momentum distributions of stable isotopes. At present, efforts are devoted to investigate with such probes highly unstable isotopes at radioactive nuclear beam (RNB) facilities. Since the first experiments [1–6], it has been found from analyses of total interaction cross sections that weakly-bound neutron-rich light nuclei, e.g., ^{6,8}He, ^{11}Li, ^{14}Be, ^{17,19}B, have increased sizes that deviate substantially from the $R \sim A^{1/3}$ rule. It was realized (e.g., Refs. [7–9]) that such a new phenomenon is due to the weak binding of the last few nucleons which form a diffuse nuclear cloud due to quantum-mechanical penetration (the so-called "nuclear halo"). Another effect is that the nucleons can form a "neutron skin" [10] when the neutrons are on average less bound than the protons. The origin of the skin lies in the large difference of the Fermi energy levels of protons and neutrons so that the neutron wave function extends beyond the effectively more bound proton wave function [9]. Thus, the term "neutron skin" describes an excess of neutrons at the nuclear surface, whereas the "halo" stands for such excess plus a long tail of the neutron density distribution.

Most exotic nuclei are so short lived that they cannot be used as targets at rest. Instead, direct reactions with RNB can be done in inverse kinematics, where the role of beam and target are interchanged. For example, proton elastic scattering angular distributions were measured at incident energies less than 100 MeV/nucleon for He isotopes (e.g., Refs. [11–20]) and Li isotopes (e.g., Refs. [9,16]) and at an energy of 700 MeV/nucleon for the same nuclei at GSI (Darmstadt) (e.g.,

Refs. [21–25]). The charge and matter distributions of these nuclei were tested in analyses of differential and total reaction cross sections of the proton scattering on exotic nuclei using different phenomenological and theoretical methods (see, Refs. [16,17,19,21–32]). It was shown (e.g., Ref. [30]) that elastic scattering of protons serves as a good tool to distinguish between different models of density distributions. It was demonstrated for the case of intermediate incident energies that proton scattering in the region of small momentum transfer is particularly sensitive to the nuclear matter radius and the halo structure of nuclei [25].

The elastic proton scattering experiments for studying the ^{6,8}He, ^{8,9,11}Li isotopes have been performed at GSI by using external targets. As noted in Ref. [25], however, the use of internal targets at storage rings in the new generation radioactive beam facilities will have advantage over external target experiments and will allow to extend such investigations to a wide range of medium and heavy nuclei.

Concerning the charge distributions of nuclei, it is known that their most accurate determination can be obtained from electron-nucleus scattering. For the case of exotic nuclei the corresponding charge densities are planned to be obtained by colliding electrons with these nuclei in storage rings. As shown in the NuPECC Report [33], a first technical proposal for a low-energy electron-heavy-ion collider made at JINR (Dubna) has been further developed and incorporated in the GSI physics program [34] along with the plan for the electron-ion collider at the MUSES facility at RIKEN [35,36]. Several interesting and challenging issues can be analyzed by the mentioned electron scattering experiments. One of them is to study how the charge distribution evolves with increasing neutron number (or isospin) at fixed proton number. The question

remains up to what extent the neutron halo or skin may trigger sizable changes of the charge root-mean-square (rms) radius, as well as of the diffuseness in the peripherical region of the charge distribution. This point may then be very important for understanding the neutron-proton interaction in the nuclear medium. To this end the preliminary theoretical calculations of the charge form factors of neutron-rich exotic nuclei can serve as a challenge for future experimental works and thus, for accurate determination of the charge distributions in these nuclei. This can be a test of the different theoretical models used for predicting charge distributions.

In recent years theoretical work has been done along these lines focusing on halo nuclei (e.g., Refs. [37–40]). In Refs. [38,39] the Borromean nuclei are described as three-body systems and the electron-ion scattering is considered in terms of a folding of a three-body density functional assuming separate interactions of electrons with the core and the halo nucleons. The three-body density functional is obtained from Faddeev calculations that employ neutron-neutron and neutron-core forces able to describe the results from collisions with heavy ions. In Ref. [40] various existing theoretical predictions for the charge distributions in light exotic nuclei ^{6,8}He, ^{11}Li, ^{14}Be, ^{17,19}B have been used for calculations of charge form factors. These were those of Tanihata *et al.* (Ref. [6] for He isotopes), the results of the cluster-orbital shell-model approximation (COSMA) (Ref. [28] for He isotopes and Ref. [16] for Li isotopes), the large-scale shell-model (LSSM) method (Ref. [41] for He isotopes and Ref. [32] for Li isotopes) and that of Suzuki *et al.* [42] for ^{14}Be and ^{17,19}B nuclei. The charge form factors have been calculated within the plane wave Born approximation. Calculations of form factors of heavier exotic nuclei within the PWBA are also presented in Refs. [43,44].

The aim of this work is as follows. Firstly, to extend in comparison with Ref. [40] the range of exotic nuclei for which charge form factors are calculated. Along with the new calculations for He and Li isotopes, we present results on charge form factors of several unstable isotopes of medium (Ni) and heavy (Kr and Sn) nuclei and compare them to those of stable isotopes in the same isotopic chain. The isotopes of Ni and Sn are chosen because they have been indicated in Refs. [35,36] as first candidates accessible for the charge densities and rms radii determination and as key isotopes for structure studies of unstable nuclei at the electron-radioactive-ion collider in RIKEN. We also give the charge densities and compare them to matter density distributions. The calculated proton, neutron, charge and matter rms radii are also presented and the latter are compared with those for ^{4,6,8}He and ^{6,11}Li deduced from the proton scattering experiments at GSI [23] and from the total interaction cross sections σ_I [1,2,4] obtained from the measurements of Tanihata *et al.* [5,6] and from the reanalysis [45,46] of the same data. In our calculations for the He and Li isotopes we do not use (in contrast to the work of Ref. [40]) the semiphenomenological densities of Tanihata and COSMA mentioned above, where the parameter values of the densities were established by a comparison with the total interaction cross sections. Both densities have unrealistic Gaussian tails at large r. Instead, we use for these nuclei the LSSM proton and neutron densities obtained in calculations based on the set of wave functions with exponential asymptotic
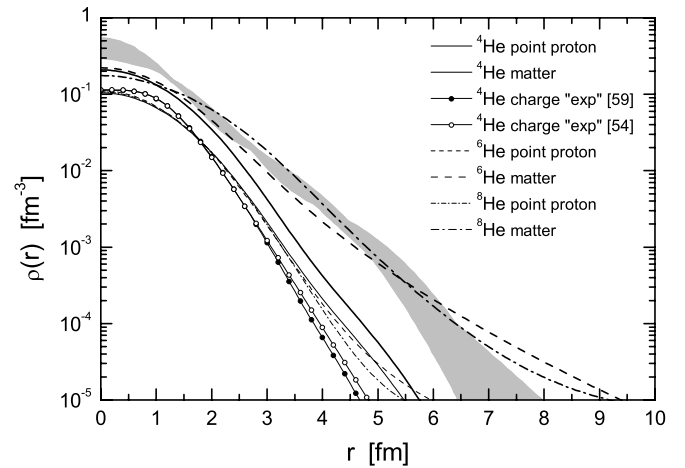

FIG. 1. Thin lines are LSSM point proton densities of ^{4,6,8}He compared to the "experimental" charge density for ^{4}He from "model-independent" analyses [54,59]. Thick lines are LSSM matter densities of ^{4,6,8}He compared to matter density of ^{8}He deduced from the experimental proton scattering cross section data in Ref. [25] (grey area).

behavior (Ref. [41] for He and Ref. [32] for Li isotopes). For the isotopes of heavier nuclei Ni, Kr, and Sn we use proton and neutron densities which are obtained from self-consistent mean-field (HF+BCS, in short HFB) calculations with density-dependent Skyrme effective interactions in a large harmonic-oscillator (HO) basis [47,48]. Secondly, in contrast to the work of Ref. [40], we calculate the charge form factors not only within the PWBA but also in DWBA by the numerical solution of the Dirac equation [49–51] for electron scattering in the Coulomb potential of the charge distribution of a given nucleus. Also, now we do not neglect neutrons, as was done in Ref. [40].
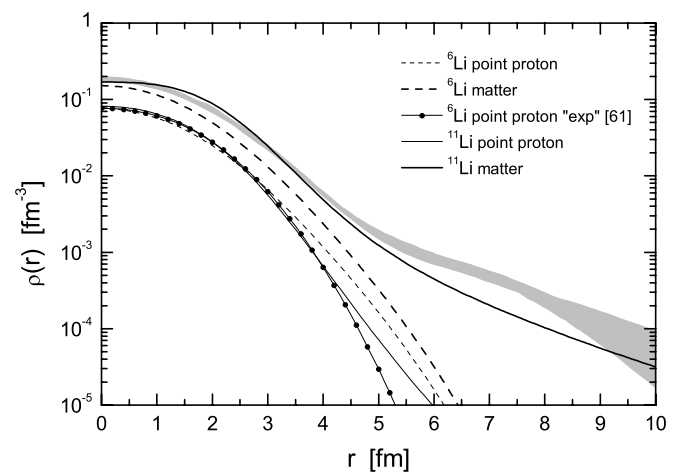

FIG. 2. Thin lines are LSSM point proton densities of ^{6,11}Li compared to the point-proton density of ^{6}Li extracted from the "experimental" charge density in a "model-independent" analysis [61]. Thick lines are LSSM matter densities of ^{6,11}Li compared to matter density of ^{11}Li deduced from the experimental proton scattering cross section data in Ref. [25] (grey area).

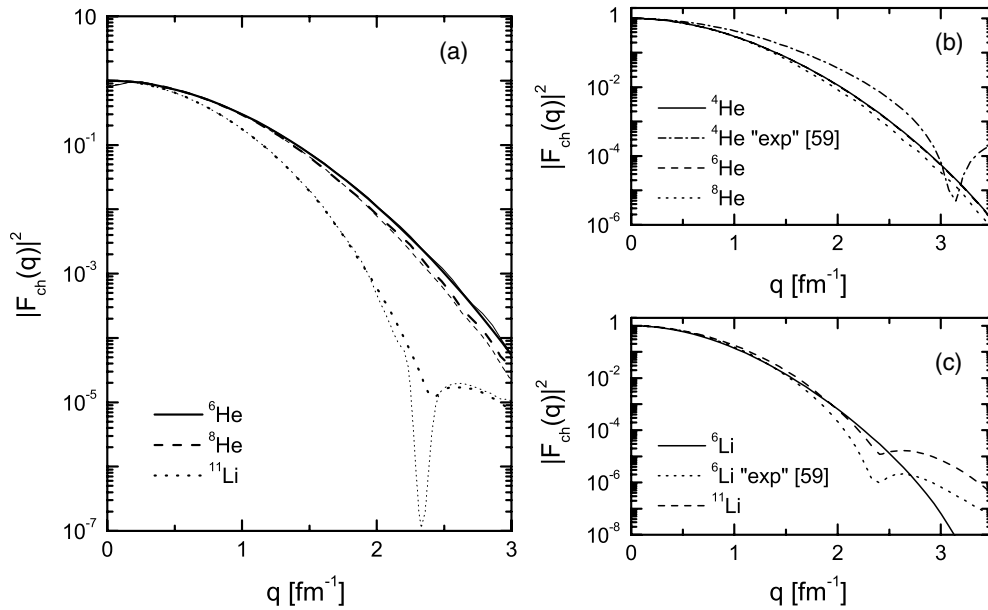FIG. 3. (a) Charge form factors of ^{6}He, ^{8}He, and ^{11}Li calculated in PWBA (thin lines) and in DWBA (thick lines) using LSSM densities; (b) charge form factors in DWBA for ^{4}He (calculated by using "experimental" charge density [59] and the LSSM density) and of ^{6,8}He (using the LSSM densities); (c) charge form factor in DWBA for ^{6}Li (using the "experimental" charge density [59] and the LSSM densities) and for ^{11}Li (using the LSSM densities).

A brief representation of the theoretical scheme is given in Sec. II. The results and discussion are given in Sec. III. The conclusions are summarized in Sec. IV.

II. THE THEORETICAL SCHEME

A. The form factors

In this section we review briefly the basic formulas used to calculate the form factors, as well as the proton and neutron densities.

The nuclear charge form factor $F_{ch}(q)$ has been calculated as follows:

$$F_{ch}(q) = \left[F_{point,p}(q) G_{Ep}(q) + \frac{N}{Z} F_{point,n}(q) G_{En}(q) \right] F_{c.m.}(q),$$

$$(1)$$

where $F_{point,p}(q)$ and $F_{point,n}(q)$ are the form factors which are related to the point-like proton and neutron densities $\rho_{point,p}(\mathbf{r})$ and $\rho_{point,n}(\mathbf{r})$, respectively. These densities correspond to wave functions in which the positions $\mathbf{r}$ of the nucleons are defined with respect to the center of the potential related to the
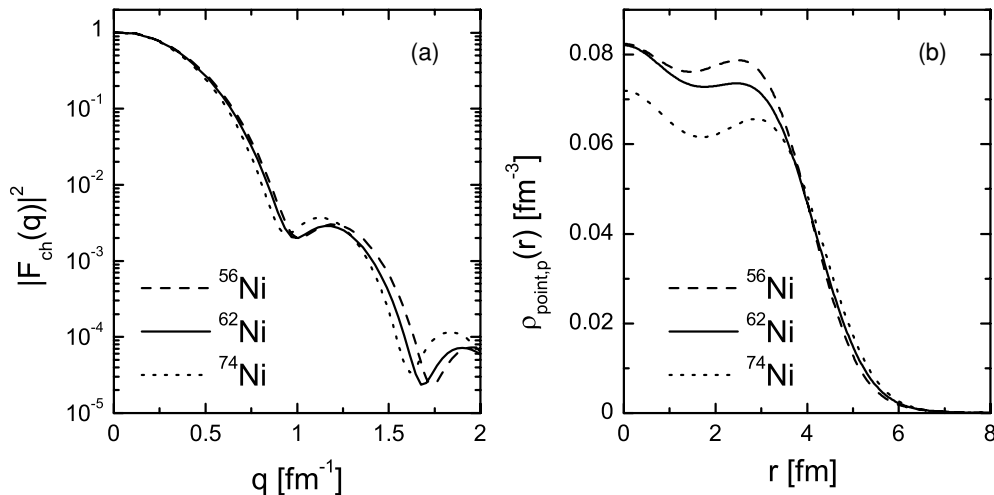

FIG. 4. (a) Charge form factors for the unstable doubly-magic ^{56}Ni, stable ^{62}Ni, and unstable ^{74}Ni isotopes calculated by using the HF+BCS densities and the DWBA; (b) HF+BCS proton densities of ^{56}Ni, ^{62}Ni, and ^{74}Ni.
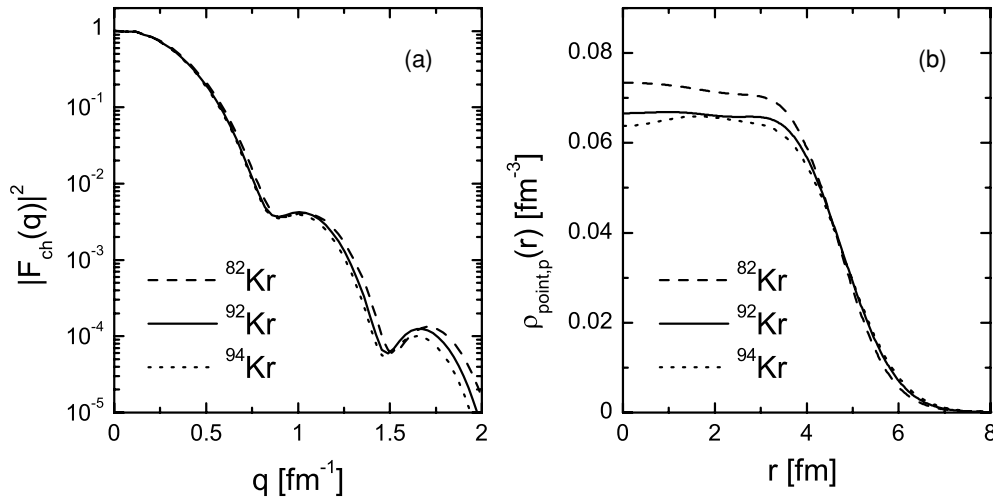
FIG. 5. (a) Charge form factors for the stable isotope ^{82}Kr and for the unstable ^{92}Kr and ^{94}Kr isotopes calculated by using the HF+BCS densities and the DWBA; (b) HF+BCS proton densities of ^{82}Kr, ^{92}Kr, and ^{94}Kr.

laboratory system. In PWBA these form factors have the form

$$F_{\text{point},p}(\mathbf{q}) = \frac{1}{Z} \int \rho_{\text{point},p}(\mathbf{r}) e^{i\mathbf{q}\mathbf{r}} d\mathbf{r} \qquad (2)$$

and

$$F_{\text{point},n}(\mathbf{q}) = \frac{1}{N} \int \rho_{\text{point},n}(\mathbf{r}) e^{i\mathbf{q}\mathbf{r}} d\mathbf{r}, \qquad (3)$$

where

$$\int \rho_{\text{point},p}(\mathbf{r}) d\mathbf{r} = Z; \qquad \int \rho_{\text{point},n}(\mathbf{r}) d\mathbf{r} = N. \qquad (4)$$

In order that $F_{\text{ch}}(q)$ corresponds to density distributions in the centre-of-mass coordinate system, a factor $F_{\text{c.m.}}(q)$ is introduced (e.g., Refs. [52–54]) in the standard way $[F_{\text{c.m.}}(q) = \exp(q^2/4A^{2/3})]$. In Eq. (1) $G_{Ep}(q)$ and $G_{En}(q)$ are the Sachs proton and neutron electric form factors, correspondingly, and they are taken from one of the most recent

phenomenological parametrizations [55]. Actually, there is no significant difference between this recent parametrization and the most traditional one of Refs. [56–58] in the range of momentum transfer considered in this work ($q < 4$ fm^{-1}).

In the present work, in addition to PWBA, we also perform DWBA calculations solving the Dirac equation which contains the central potential arising from the proton ground-state distribution. We use two codes for the numerical calculations of the form factors: (i) that of Ref. [50] which follows Ref. [49] and (ii) the code from Ref. [51]. The results of both calculations were found in good agreement.

B. The density distributions

The theoretical predictions for the point-like proton and neutron nuclear densities of the light exotic nuclei ^{6,8}He and ^{11}Li, as well as of the corresponding stable isotopes

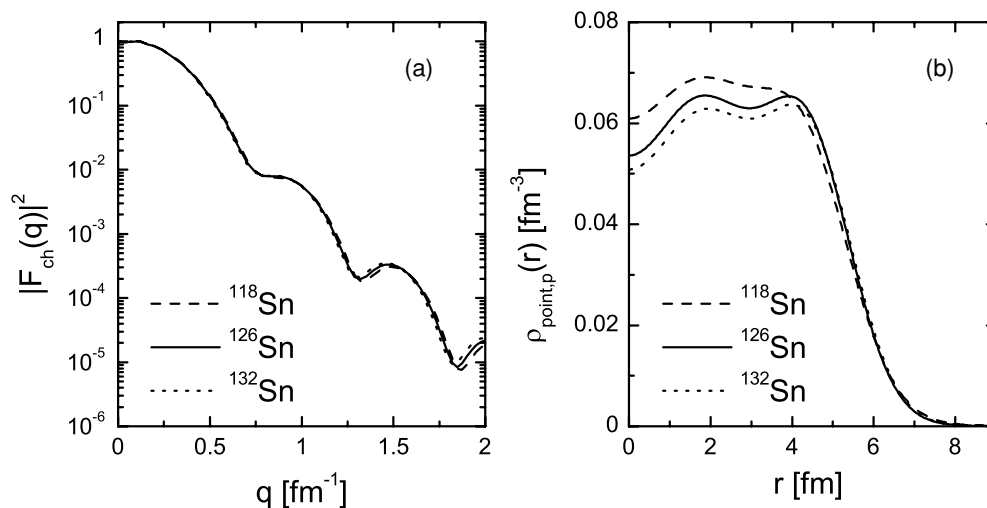FIG. 6. (a) Charge form factors for the stable isotope ^{118}Sn, unstable ^{126}Sn, and unstable doubly-magic ^{132}Sn isotopes calculated by using the HF+BCS densities and the DWBA; (b) HF+BCS proton densities of ^{118}Sn, ^{126}Sn, and ^{132}Sn.
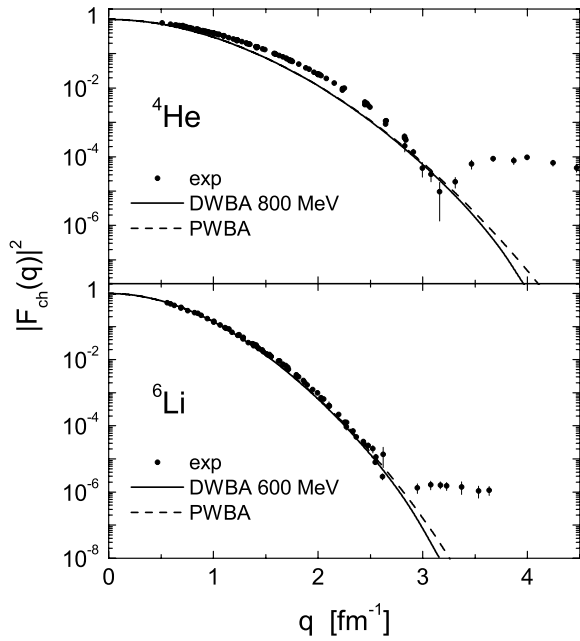
FIG. 7. Charge form factors for the stable isotopes ^{4}He and ^{6}Li calculated using LSSM densities in PWBA and in DWBA in comparison with the experimental data.

^{4}He and ^{6}Li are taken from the LSSM calculations. For ^{4,6,8}He nuclei they are obtained in a complete $4\hbar\omega$ shell-model space [41]. The LSSM calculations use a Woods-Saxon single-particle wave function basis for ^{6}He and ^{8}He and HO one for ^{4}He. For comparison we use also the "experimental" charge density for ^{4}He [54,59,60], i.e., the so-called "model-independent" shape of the density. The proton and neutron
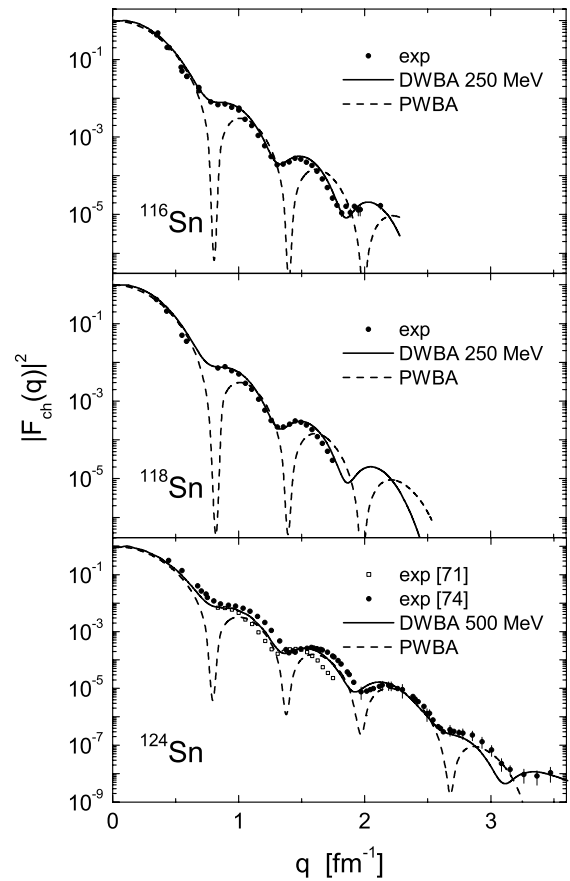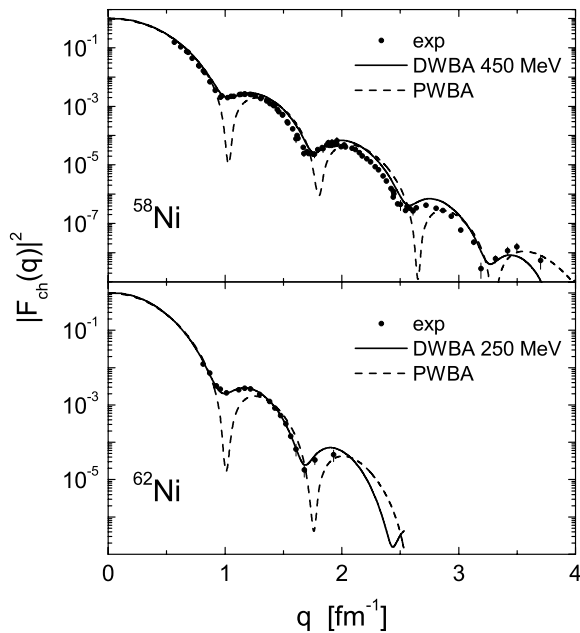

FIG. 8. Charge form factors for the stable isotopes ^{58}Ni and ^{62}Ni calculated by using the HF+BCS densities and the PWBA and DWBA in comparison with the experimental data.

FIG. 9. Charge form factors for the stable isotopes ^{116}Sn, ^{118}Sn, and ^{124}Sn calculated by using the HF+BCS densities and the PWBA and DWBA in comparison with the experimental data.

densities of ^{6}Li are obtained within the LSSM in a complete $4\hbar\omega$ shell-model space and of ^{11}Li in complete $2\hbar\omega$ shell-model calculations [32]. For ^{6}Li the single-particle HO wave functions have been used in the LSSM calculations and Woods-Saxon ones for ^{11}Li. For ^{6}Li we also use the point-proton nuclear density distribution taken from Refs. [61,62] which leads to the "experimental" charge distribution with rms radius equal to 2.57 fm [61].

The point proton and neutron density distributions of Ni, Kr, and Sn isotopes are taken from deformed self-consistent HFB calculations with density-dependent SG2 effective interactions using a large HO basis with 11 major shells [48,63].

III. RESULTS AND DISCUSSION

We calculate charge form factors for a variety of exotic nuclei with both PWBA and DWBA. As mentioned above, the proton and neutron densities used for He and Li isotopes are obtained from realistic microscopic calculations with the LSSM method [32,41], while the densities used for Ni, Kr, and Sn isotopes are calculated in the deformed self-consistent HF+BCS method.

Let us first discuss the light nuclei. We show in Figs. 1 and 2 the point proton and matter density distributions (normalized correspondingly to Z and A) calculated with LSSM for the

He isotopes ^{4,6,8}He [41] and Li isotopes ^{6,11}Li [32]. Matter distribution is taken to be $\rho_m(r) = \rho_{\text{point},p}(r) + \rho_{\text{point},n}(r)$. In addition, for the sake of completeness of the comparison we give the "experimental" charge density of the stable isotope ^{4}He (in Fig. 1) [54,59] and the point-proton density of the ^{6}Li nucleus (in Fig. 2) extracted from the "experimental" charge density in Ref. [61].

Firstly, one can see from Fig. 1 the considerable difference between the "experimental" charge density of ^{4}He and the point proton densities of ^{4,6,8}He calculated in LSSM which is also informative of the role of the charge distribution of the proton itself. Secondly, the differences between the LSSM proton density of ^{4}He and those of ^{6}He and ^{8}He are not so large. The only change occurs in the high-r tail, mainly due to the different (HO versus Woods-Saxon) basis used in the LSSM calculations of ^{4}He. Much more noticeable, however, is the difference between the LSSM point proton densities in ^{6}Li and ^{11}Li seen in Fig. 2. There is also a difference at large values of r between the LSSM proton density of ^{6}Li and the point-proton density of the same nucleus extracted from the "experimental" charge density in a "model-independent" analysis [61]. As expected, the matter distributions of neutron-rich ^{6,8}He and ^{11}Li are quite different from those of the stable ^{4}He and ^{6}Li both in the surface region and in the interior of nuclei.

For comparison we present by grey area also the matter densities of ^{8}He (in Fig. 1) and ^{11}Li (in Fig. 2) deduced from the experimental data for the differential cross sections of elastic proton scattering at small momentum transfer which have been measured at GSI at energies around 700 MeV/nucleon in inverse kinematics for neutron-rich helium and lithium isotopes [25]. A model-dependent method to extract the matter distributions was used for these nuclei exploring various parametrizations for the nucleon density distributions. The calculated LSSM matter distribution for ^{8}He is in agreement with that extracted from proton scattering data [25] in the interval $2 \leqslant r \leqslant 7$ fm. For ^{11}Li this is the case in the interval $0 \leqslant r \leqslant 4$ fm.

In Fig. 3(a) the results for the charge form factors [Eq. (1)] of ^{6,8}He and ^{11}Li obtained in PWBA (thin lines) and in DWBA (thick lines) using LSSM densities are shown. In Fig. 3(b) the charge form factors of ^{4}He obtained in DWBA by means of the "experimental" [59] and LSSM charge density are compared with those of ^{6}He and ^{8}He. The same is shown in Fig. 3(c) for the ^{6}Li nucleus in comparison with the form factor of ^{11}Li (using its LSSM densities). The DWBA calculations are performed at an energy of 540 MeV. One can see from Fig. 3(a) the small difference of the charge form factors of ^{6}He and ^{8}He at $q \geqslant 1$ fm^{-1} and the small deviation of the DWBA from PWBA results in the whole q-range. It is shown in Fig. 3(b) the similarity of the LSSM charge form factors of ^{4}He and ^{6}He and their difference from that of ^{8}He. At the same time there is not a minimum in this q-range in all three LSSM form factors of ^{4,6,8}He in contrast to the case for the "experimental" charge form factor of ^{4}He.

In Figs. 4, 5, and 6 we present the charge form factors calculated with DWBA at an energy of 250 MeV as well as the HF+BCS proton densities for ^{56,62,74}Ni, ^{82,92,94}Kr, and ^{118,126,132}Sn, correspondingly. A common feature of the charge form factors of the Ni, Kr, and Sn isotopes considered, which can be seen in Figs. 4(a), 5(a), and 6(a), is the shift of the minima to smaller values of q when the number of neutrons increases in a given isotopic chain. This is due mainly to the enhancement of the proton densities in the peripherical region and also (to a minor extent) to the contribution of the charge distribution of the neutrons themselves. Indeed, one can see from Figs. 4(b), 5(b), and 6(b) that the point proton densities in a given isotopic chain decrease in the central region and increase in the surface with increasing neutron number.

The isotopic sensitivities of the calculated charge form factors to the changes of neutron number observed in Figs. 4(a), 5(a), and 6(a) and their precise measuring in future electron-nucleus scattering experiments may lead to accurate determination of charge distributions for unstable nuclei. The techniques used to extract charge distributions

FIG. 10. (a) Charge form factors for the stable isotope ^{118}Sn calculated by using the DWBA (thick solid line), PWBA (dashed line), and PWIA with q_{eff} given in the text (thin solid line); (b) Charge form factor for the unstable doubly-magic ^{132}Sn isotope calculated by using the DWBA and corresponding to Eq. (1) (solid line) and to the proton contribution only [i.e., to the first term of Eq. (1)] (dashed line).

TABLE I. Proton (R_p), neutron (R_n), charge (R_{ch}), matter (R_m) rms radii (in fm), and difference $\Delta R = R_m - R_p$ of He and Li isotopes calculated using LSSM densities. Available data on R_m and R_{ch} are also presented.

Nuclei	R_p	R_n	R_{ch}	R_m	ΔR	R_m [23]	R_m [5,6]	R_m [45,46]	R_{ch} [59,61]	R_{ch} [54]
[4]He	1.927	1.927	2.153	1.927	0.000	1.49(3)			1.696(14)	1.695
[6]He	1.945	2.900	2.147	2.621	0.676	2.30(7)	2.33(4)	2.54(4)		
[8]He	1.924	2.876	2.140	2.670	0.746	2.45(7)	2.49(4)			
[6]Li	2.431	2.431	2.647	2.431	0.000	2.45(7)	2.32(3)		2.57(10)	2.539
[11]Li	2.238	3.169	2.477	2.945	0.707	3.62(19)	3.12(16)	3.53(10)		

from the measured elastic form factors are well established. For instance, the model-dependent method in which the direct scattering problem is solved parametrizing the charge distribution and the respective parameters are fitted to the experimental cross sections, has been demonstrated in Ref. [64] to show the sensitivity of the cross section (and of the charge form factor, respectively) to variations in radius and diffuseness parameters. The data were simulated for the ^{132}Sn(e, e) elastic scattering at a luminosity of 10^{28} cm^{-2} s^{-1}. This model estimation shows that at low-momentum transfers ($q < 1.5$ fm^{-1}) the charge form factor of ^{132}Sn can be precisely measured. However, in the range of moderate- and high-momentum transfer, where the charge form factor is dominated by the details of the charge density distribution, the expected error band becomes appreciable. Hence, covering a wider region of q makes possible to determine the charge distribution but requires higher luminosities. There is a qualitative agreement of model-dependent calculations of charge form factors for Sn nucleus in Ref. [35] with our results shown in Fig. 6(a). Another way to extract the charge distributions is to use a model-independent analysis based upon the expansion of the charge density on a complete set of orthogonal functions. Such type of analysis allows one to show whether the isotopic effects on charge densities can be measured convincingly. Since the charge distribution of unstable nuclei is the main subject of the coming experiments at next-generation electron-nucleus colliders, this problem deserves further study.

For the sake of completeness we show the comparison of the DWBA results with available experimental data for the charge form factors of the isotopes ^{4}He [65,66] and ^{6}Li [67,68] (Fig. 7), ^{58}Ni [69] and ^{62}Ni [70] (Fig. 8), ^{116}Sn [71–73], ^{118}Sn [71,72] and ^{124}Sn [71,74] (Fig. 9). Our DWBA calculations are performed at the electron energies used in the experiments. The agreement with the empirical data for the stable isotopes is supportive of our results on the exotic nuclei to be used as guidance to future experiments particularly so on the medium-heavy and heavy ones. A common feature is the expected filling of the Born zeros when DWBA is used (instead of PWBA), as well as the shift of the minima to smaller values of q and the increase of the secondary peaks which can be seen in Figs. 8 and 9.

In this spirit we would also like to note that the displacement to the left of the DWBA calculations versus PWBA can be accounted for by replacement of the momentum transfer q with the effective momentum transfer $q_{\rm eff}$ (see, e.g., Ref. [75]). We take into account this correction (which is due to the Coulomb attraction felt by the electrons) by using $q_{\rm eff} = q[1 + (cZ\alpha/R_{\rm ch}E_i)]$, where the constant c (in our work $c = 1$) is related to the charge rms radii $R_{\rm ch}$ obtained in the present calculations. The effect of using $q_{\rm eff}$ is clearly seen in Fig. 10(a) on the example of ^{118}Sn isotope. It describes the shift of the minima produced by the Coulomb distortion of the electron waves. To illustrate the effect of the neutron form factor on the nuclear charge form factor, we show in Fig. 10(b) for the case of ^{132}Sn the results corresponding to the total charge form factor $F_{\rm ch}(q)$ as defined in Eq. (1) and to its proton contribution $F_{{\rm point},p}(q)G_{Ep}(q)$. As can be seen from the figure, although the contribution from the neutrons is rather small (around 10–20%

TABLE II. Proton (R_p), neutron (R_n), charge (R_{ch}), matter (R_m) rms radii (in fm), and difference $\Delta R = R_m - R_p$ of Ni, Kr, and Sn isotopes calculated using HF+BCS densities. The last two columns present experimental data on R_{ch}.

Nuclei	R_p	R_n	R_{ch}	R_m	ΔR	R_{ch} [61]	R_{ch} [76]
[56]Ni	3.725	3.666	3.795	3.696	−0.029		
[58]Ni	3.719	3.697	3.794	3.707	−0.012	3.764(10)	
[62]Ni	3.798	3.855	3.866	3.829	0.031	3.830(13)	
[74]Ni	3.911	4.130	3.977	4.049	0.138		
[82]Kr	4.126	4.190	4.189	4.162	0.036		4.192(4)
[92]Kr	4.224	4.412	4.285	4.340	0.116		4.273(16)
[94]Kr	4.277	4.496	4.338	4.413	0.136		4.300(20)
[116]Sn	4.583	4.650	4.646	4.621	0.038	4.626(15)	
[118]Sn	4.649	4.739	4.705	4.701	0.052	4.679(16)	
[126]Sn	4.642	4.798	4.698	4.737	0.095		
[132]Sn	4.685	4.879	4.740	4.807	0.122		

TABLE III. Diffuseness parameter values (in fm) of the LSSM densities of He and Li isotopes and HF+BCS densities of Ni, Kr, and Sn isotopes considered in this work.

Nuclei	a_p	a_n	a_m	a_{ch}
[4]He	0.407	0.407	0.407	0.392
[6]He	0.397	0.498	0.448	0.381
[8]He	0.403	0.513	0.549	0.387
[6]Li	0.521	0.521	0.521	0.509
[11]Li	0.482	0.444	0.493	0.478
[56]Ni	0.484	0.505	0.493	0.527
[62]Ni	0.920	0.557	0.572	0.616
[74]Ni	0.538	0.445	0.475	0.552
[82]Kr	0.509	0.459	0.477	0.570
[92]Kr	0.505	0.541	0.527	0.564
[94]Kr	0.516	0.761	0.639	0.582
[118]Sn	0.468	0.555	0.509	0.534
[126]Sn	0.382	0.707	0.482	0.445
[132]Sn	0.377	0.698	0.473	0.434

in the q-range 1.5–2 fm^{-1}), it is comparable in size to the isotopic effect and, therefore, should not be neglected.

We would like to note the reasonable agreement of the results of the DWBA calculations with the experimental charge form factors of the isotopes of Ni and Sn considered. The lack of theoretical minima for [4]He and [6]Li, however, leads us to the conclusion that the LSSM densities of these light stable isotopes do not seem reliable. The latter might be due to the use of harmonic-oscillator wave functions in the LSSM calculations for these nuclei.

In Tables I and II we give the rms radii (R_p, R_n, R_{ch}, R_m) corresponding to nuclear proton, neutron, charge, and matter distributions, as well as the difference $\Delta R = R_m - R_p$ for the He and Li isotopes (Table I) and for the Ni, Kr, and Sn isotopes (Table II) which are considered in our work. The values of the diffuseness parameter of the various densities are presented in Table III. The diffuseness parameter is defined as the distance

over which the value of the density decreases in the surface region from 90% to 10% of its value in the center of the nucleus divided by 4.4. For comparison we give additionally in Table I the nuclear matter radii of [4]He, [6]He, [8]He, and [6]Li, [11]Li deduced from the proton scattering experiments at GSI [23], from the data on total interaction cross sections σ_I [1,2,4] obtained from an analysis of Tanihata *et al.* [5,6] and from a more recent reanalysis [45,46] of the same data. We present in Table I for a comparison also the experimental charge rms radii for [4]He and [6]Li from [54,59,61] and in Table II those for [58,62]Ni and [116,118]Sn from [61] and for [82,92,94]Kr from [76].

It is seen from Table I that the calculated rms radii of He and Li isotopes follow the behavior of the density distributions shown in Figs. 1 and 2. One can also see that the calculated charge rms radii of [4]He and [6]Li are larger than the experimental ones as could have been foreseen from Figs. 3(a) and 3(c). The matter density of [11]Li exhibits the most extended halo component (see Fig. 2) among all helium and lithium isotopes being investigated, which is reflected in large neutron radius $R_n = 3.169$ fm and, correspondingly, in large matter radius $R_m = 2.945$ fm. The nuclei [6]He and [8]He have less extended nuclear matter distributions than [11]Li (see Fig. 1) and thus smaller matter radii, $R_m = 2.621$ fm and $R_m = 2.670$ fm compared to 2.945 fm in [11]Li. Our theoretically calculated R_m for [6]He is in closer agreement with the value from the reanalysis of the data deduced from total interaction cross sections [5] performed by Al-Khalili *et al.* [45]. As for [6]Li, the result from the present calculation exceeds the value $R_m = 2.32(3)$ fm from Tanihata *et al.* [5], but almost coincides with the value $R_m = 2.45(7)$ fm deduced from the recent proton scattering experiments at GSI [23].

The common tendency of all predicted rms radii for medium (Ni) and heavy (Kr and Sn) nuclei presented in Table II is the small increase of their values with the increase of the number of neutrons in a given isotopic chain except that R_{ch} of [126]Sn is practically the same as R_{ch} of [118]Sn. Our theoretical results on R_{ch} in Table II are in good agreement with the available experimental values [61,76]. A more detailed study of the
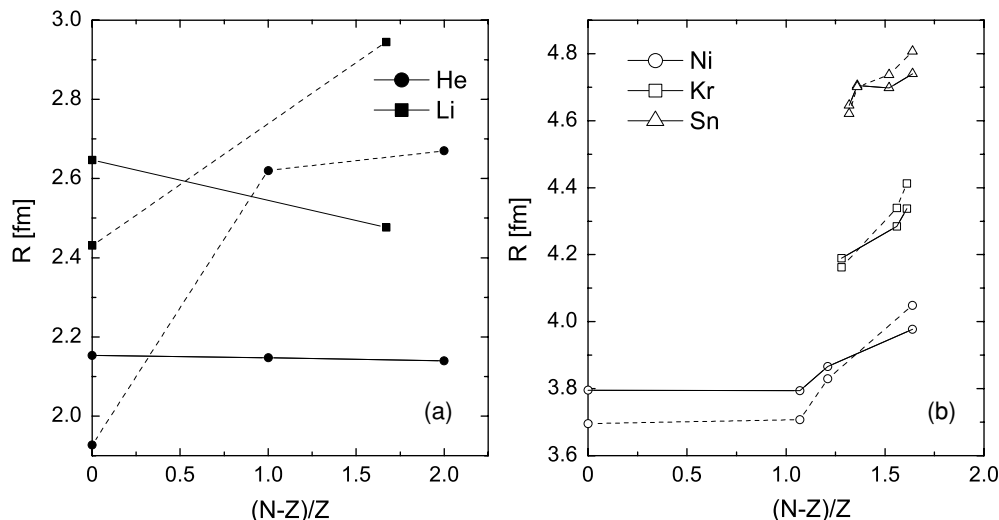

FIG. 11. Charge (R_{ch}) (solid lines to guide the eye) and matter (R_m) (dashed lines) rms radii calculated in this work as a function of the relative neutron excess $(N - Z)/Z$ of He and Li isotopes (full symbols) (a) and Ni, Kr, and Sn isotopes (open symbols) (b).

rms radii of these nuclei is required when future experiments will be performed. In particular, the charge rms radius can be determined using the model-independent relation of the form factor in the lower q-region (e.g., Ref. [77]),

$$R_{ch}^2 = -6 \left[\frac{dF_{ch}(q^2)}{d(q^2)} \right]_{q^2=0}. \tag{5}$$

In our opinion, the calculated difference $\Delta R = R_m - R_p$ whose values are listed also in Tables I and II is of particular importance and together with the neutron thickness $R_n - R_p$ presented in Refs. [78,79] can serve as a measure of the halo or neutron skin structure of neutron-rich exotic nuclei.

In addition, we show in Fig. 11 the variation of the charge and matter rms radii with the relative neutron excess for all isotopic chains considered. The use of LSSM charge densities for He and Li isotopes [32,41] leads to a small decrease of the charge rms radius R_{ch} from ^{4}He to ^{6}He and ^{8}He and to a larger decrease of R_{ch} from ^{6}Li to ^{11}Li. On the contrary, the behavior of the charge radii for heavier Ni, Kr, and Sn isotopes shows a smooth increase of R_{ch} with increase of the neutron number, while the nuclear matter radii for these isotopes increase faster. In order to test the theoretical predictions for the charge and matter radii, it is desirable to measure both matter and charge distributions for the same nuclei. The difference in size of these distributions will be of high interest and importance for the theoretical understanding of the exotic nuclei structure.

IV. CONCLUSIONS

In this work we extended the studies of the previous one [40] of the proton, neutron, charge, and matter densities and related charge form factors from the light neutron-rich exotic nuclei ^{6,8}He, ^{11}Li to examples of unstable medium (Ni) and heavy (Kr and Sn) isotopes in comparison with those of stable isotopes in the same isotopic chain. For He and Li isotopes we use the proton and neutron densities obtained from realistic microscopic calculations within the large-scale shell-model method [32,41]. The densities of Ni, Kr, and Sn isotopes are calculated in HF+BCS method with a density-dependent effective interaction using a large harmonic-oscillator basis [47,48].

We also compare proton and matter density distributions for He and Li isotopes. The calculated matter distributions for the halo nuclei are much more extended than the proton ones. We compare proton density distributions for the isotopes of He, Li, Ni, Kr, and Sn and establish the differences of the proton densities in a given isotopic chain due to the presence of the neutron excess. There is a decrease of the proton density in the nuclear interior and an increase of its tail at large r with increasing neutron number.

A comparison of the proton, neutron, charge, and matter rms radii as well as the corresponding diffuseness is performed for all isotopic chains considered. We point out that the general trend of the difference ΔR between the matter and proton rms radii is to increase with the number of neutrons but for the heavy isotopes this increase is moderate compared to that of the light ones.

The calculated matter densities for ^{8}He and ^{11}Li are in fair agreement with the experimental data obtained in proton scattering on these isotopes in GSI [23]. We compare the matter rms radii with those from Ref. [23] as well as with those from total interaction cross section data [1,2,4,6] and their reanalysis [45,46].

We calculate the charge form factors of He, Li, Ni, Kr, and Sn isotopes by means of the densities mentioned above. The charge form factors are calculated not only in the PWBA as in our previous work [40] but also in the DWBA, solving the Dirac equation for electron scattering in the Coulomb potential of the charge distribution in a given nucleus. By accounting for the Coulomb distortion of the electron waves the Born zeros are filled and the form factors are shifted to smaller values of q which is clearly seen in the cases of the Ni, Kr, and Sn isotopes where Z is large enough. We find that this shift is best parametrized by $q_{eff} = q[1 + (Z\alpha/R_{ch}E_i)]$, where R_{ch} are the charge rms radii as given in the tables. In addition we also take into account the charge distribution in the neutron itself. We find that the contributions from the neutrons to the charge form factors are less than 20% up to $q \sim 2$ fm^{-1}.

The differences between the charge form factors in a given isotopic chain are shown. The common feature of the charge form factors is the shift of the form factor curves and their minima to smaller values of q with the increase of the neutron number in a given isotopic chain. This is due to the corresponding enhancement of the proton tails in the peripherical region of the nuclei.

The performed theoretical analyses of the densities and charge form factors can be a step in the studies of the influence of the increasing neutron number on the proton and charge distributions in a given isotopic chain. This is important for understanding the neutron-proton interaction in the nuclear medium. We emphasize also the questions of interest, namely, the necessary both kinematical regions of the proposed experiments and precision to measure small shifts in the form factors.

The theoretical predictions for the charge form factors of exotic nuclei are a challenge for their measurements in the future experiments in GSI and RIKEN and thus, for obtaining detailed information on the charge distributions of such nuclei. The comparison of the calculated charge form factors with the future data will be a test of the corresponding theoretical models used for studies of the exotic nuclei structure.

[1] I. Tanihata, H. Hamagaki, O. Hashimoto, S. Nagamiya, Y. Shida, N. Yoshikawa, O. Yamakawa, K. Sugimoto, T. Kobayashi, D. E. Greiner, N. Takahashi, and Y. Nojiri, Phys. Lett. **B160**, 380 (1985).

[2] I. Tanihata, H. Hamagaki, O. Hashimoto, Y. Shida, N. Yoshikawa, K. Sugimoto, O. Yamakawa, and T. Kobayashi, Phys. Rev. Lett. **55**, 2676 (1985).

[3] I. Tanihata, Prog. Part. Nucl. Phys. **35**, 505 (1985).

[4] I. Tanihata, Nucl. Phys. **A488**, 113c (1988).

[5] I. Tanihata, T. Kobayashi, O. Yamakawa, S. Shimoura, K. Ekuni, K. Sugimoto, N. Takahashi, T. Shimoda, and H. Sato, Phys. Lett. **B206**, 592 (1988).

[6] I. Tanihata, D. Hirata, T. Kobayashi, S. Shimoura, K. Sugimoto, and H. Toki, Phys. Lett. **B289**, 261 (1992).

[7] P. G. Hansen, A. S. Jensen, and B. Jonson, Annu. Rev. Nucl. Sci. **45**, 591 (1995).

[8] J. Dobaczewski, I. Hamamoto, W. Nazarewicz, and J. A. Sheikh, Phys. Rev. Lett. **72**, 981 (1994).

[9] R. F. Casten and B. M. Sherill, Prog. Part. Nucl. Phys. **45**, S171 (2000), see also the special issue of Nucl. Phys. **A693**, 1 (2001).

[10] I. Tanihata, Prog. Part. Nucl. Phys. **35**, 505 (1995).

[11] Yu. T. Oganessian, V. I. Zagrebaev, and J. S. Vaagen, Phys. Rev. Lett. **82**, 4996 (1999).

[12] Yu. T. Oganessian, V. I. Zagrebaev, and J. S. Vaagen, Phys. Rev. C **60**, 044605 (1999).

[13] M. D. Cortina-Gil, P. Roussel-Chomaz, N. Alamanas, J. Barette, W. Mittig, F. Auger, Y. Blumenfeld, J. M. Casandjian, M. Chartier, V. Fekou-Youmbi, B. Fernandez, N. Frascaria, A. Gillibert, H. Laurent, A. Lepine-Szily, N. A. Orr, V. Pascalon, J. A. Scarpaci, J. L. Sida, and T. Saomijarvi, Nucl. Phys. **A616**, 215c (1997).

[14] A. Lagoyannis, F. Auger, A. Mussumara, N. Alamanos, E. C. Polacco, A. Pakou, Y. Blumenfeld, F. Braga, M. L. Commara, A. Drouart, G. Fioni, A. Gillebert, E. Khan, V. Lapoux, W. Mittig, S. Ottini-Hustache, D. Pierroutsakou, M. Romoli, P. Roussel-Chomaz, M. Sandoli, D. Santonocito, J. A. Scarpaci, J. L. Sida, T. Saomijarvi, S. Karataglidis, and K. Amos, Phys. Lett. **B518**, 27 (2001).

[15] M. D. Cortina-Gil, P. Roussel-Chomaz, N. Alamanas, J. Barette, W. Mittig, F. Auger, Y. Blumenfeld, J. M. Casandjian, M. Chartier, V. Fekou-Youmbi, B. Fernandez, N. Frascaria, A. Gillibert, H. Laurent, A. Lepine-Szily, N. A. Orr, V. Pascalon, J. A. Scarpaci, J. L. Sida, and T. Saomijarvi, Phys. Lett. **B371**, 14 (1996).

[16] A. A. Korsheninnikov, E. A. Kuzmin, E. Yu. Nikolskii, C. A. Bertulani, O. V. Bochkarev, S. Fukuda, T. Kobayashi, S. Momota, B. G. Novatskii, A. A. Ogloblin, A. Ozawa, V. Pribora, I. Tanihata, and K. Yoshida, Nucl. Phys. **A616**, 189c (1997).

[17] A. A. Korsheninnikov, E. Yu. Nikolskii, C. A. Bertulani, S. Fukuda, T. Kobayashi, E. A. Kuzmin, S. Momota, B. G. Novatskii, A. A. Ogloblin, A. Ozawa, V. Pribora, I. Tanihata, and K. Yoshida, Nucl. Phys. **A617**, 45 (1997).

[18] G. M. Ter-Akopian *et al.*, in *Fundamental Issues in Elementary*, *Proceedings of the Symposium on Honor and Memory of Michael Danos, Bad Honnef, Germany, 2000*, edited by W. Greiner (EP Systema, Debrecen, 2001), p. 371.

[19] L. L. Chulkov, C. A. Bertulani, and A. A. Korsheninnikov, Nucl. Phys. **A587**, 291 (1995).

[20] A. A. Korsheninnikov, K. Yoshida, D. V. Alexandrov, N. Aoi, Y. Doki, N. Inabe, M. Fujimaki, T. Kobayashi, H. Kumagai, C.-B. Moon, E. Yu. Nikolskii, M. M. Obuti, A. A. Ogloblin, A. Ozawa, S. Shimoura, Y. Watanabe, and M. Yanokura, Phys. Lett. **B316**, 38 (1993).

[21] G. D. Alkhazov, A. V. Dobrovolsky, P. Edelhof, H. Geissel, H. Irnich, A. V. Khanzadeev, G. A. Korolev, A. A. Lobodenko, G. Münzenberg, M. Mutterer, S. R. Neumaier, W. Schwab, D. M. Selivestrov, T. Suzuki, and A. A. Vorobyov, Nucl. Phys. **A712**, 269 (2002).

[22] P. Egelhof, Prog. Part. Nucl. Phys. **46**, 307 (2001).

[23] P. Egelhof *et al.*, Eur. Phys. J. A **15**, 27 (2002).

[24] S. R. Neumeier *et al.*, Nucl. Phys. **A712**, 247 (2002).

[25] P. Egelhof, O. Kisselev, G. Münzenberg, S. R. Neumeier, and H. Weick, Phys. Scr. T **104**, 151 (2003), and references therein.

[26] R. Crespo, J. A. Tostevin, and R. C. Johnson, Phys. Rev. C **51**, 3283 (1995).

[27] M. V. Zhukov, B. V. Danilin, D. V. Fedorov, J. M. Bang, I. J. Thompson, and J. S. Vaagen, Phys. Rep. **231**, 151 (1993).

[28] M. V. Zhukov, A. A. Korsheninnikov, and M. H. Smedberg, Phys. Rev. C **50**, 1(R) (1994).

[29] M. Avrigeanu, G. S. Anagnostatos, A. N. Antonov, and J. Giapitzakis, Phys. Rev. C **62**, 017001 (2000).

[30] M. Avrigeanu, G. S. Anagnostatos, A. N. Antonov, and V. Avrigeanu, Int. J. Mod. Phys. E **11**, 249 (2002).

[31] P. J. Dortmans, K. Amos, S. Karataglidis, and J. Rainal, Phys. Rev. C **58**, 2249 (1998).

[32] S. Karataglidis, B. A. Brown, K. Amos, and P. J. Dortmans, Phys. Rev. C **55**, 2826 (1997).

[33] Radioactive Nuclear Beam Facilities, NuPECC Report, Europe, 2000.

[34] Electromagnetic Probes and the Structure of Hadrons and Nuclei, Prog. Part. Nucl. Phys. **44** (2000); G. Shrieder *et al.*, Proposal for GSI RI Beam Factory, 2001.

[35] T. Suda, in *Challenges of Nuclear Structure*, Proceedings of the 7th International Spring Seminar on Nuclear Physics, edited by Aldo Covello (World Scientific Publishing Co., Singapore, 2002), p. 13; Proposal for RIKEN RI Beam Factory, 2001.

[36] T. Katayama, T. Suda, and I. Tanihata, Phys. Scr. T **104**, 129 (2003).

[37] E. Garrido and E. Moya de Guerra, Nucl. Phys. **A650**, 387 (1999).

[38] E. Garrido and E. Moya de Guerra, Phys. Lett. **B488**, 68 (2000).

[39] E. Moya de Guerra, E. Garrido, and P. Sarriguren, in *Challenges of Nuclear Structure*, Proceedings of the 7th International Spring Seminar on Nuclear Physics, edited by Aldo Covello (World Scientific Publishing Co., Singapore, 2002), p. 63.

[40] A. N. Antonov, M. K. Gaidarov, D. N. Kadrev, P. E. Hodgson, and E. Moya de Guerra, Int. J. Mod. Phys. E **13**, 759 (2004).

[41] S. Karataglidis, P. J. Dortmans, K. Amos, and C. Bennhold, Phys. Rev. C **61**, 024319 (2000).

[42] T. Suzuki, R. Kanungo, O. Bochkarev, L. Chulkov, D. Cortina, M. Fukuda, H. Geissel, M. Hellström, M. Ivanov, R. Janik, K. Kimura, T. Kobayashi, A. A. Korsheninnikov, G. Münzenberg, F. Nickel, A. A. Ogloblin, A. Ozawa, M. Pfützner, V. Pribora, H. Simon, B. Sitàr, P. Strmen, K. Sumiyoshi, K. Summerer, I. Tanihata, M. Winkler, and K. Yoshida, Nucl. Phys. **A658**, 313 (1999).

[43] Z. Wang and Z. Ren, Phys. Rev. C **70**, 034303 (2004); **71**, 054323 (2005).

[44] W. A. Richter and B. A. Brown, Phys. Rev. C **67**, 034317 (2003).

[45] J. S. Al-Khalili, J. A. Tostevin, and I. J. Thompson, Phys. Rev. C **54**, 1843 (1996).

[46] J. A. Tostevin and J. S. Al-Khalili, Nucl. Phys. **A616**, 418c (1997).

[47] P. Sarriguren *et al.*, in preparation.

[48] P. Sarriguren, E. Moya de Guerra, and A. Escuderos, Nucl. Phys. **A658**, 13 (1999).

[49] D. R. Yennie, D. G. Ravenhall, and R. N. Wilson, Phys. Rev. **95**, 500 (1954), and references therein.

[50] V. K. Lukyanov, E. V. Zemlyanaya, D. N. Kadrev, A. N. Antonov, K. Spasova, G. S. Anagnostatos, and J. Giapitzakis, Part. Nucl. Lett. **2[111]**, 5 (2002); Bull. Rus. Acad. Sci. Phys. **67**, 790 (2003).

[51] M. Nishimura, E. Moya de Guerra, and D. W. L. Sprung, Nucl. Phys. **A435**, 523 (1985); J. M. Udias, M.Sc. thesis, Universidad Autonoma de Madrid (unpublished) (1987).

[52] T. de Forest, Jr., and J. D. Walecka, Adv. Phys. **15**, 1 (1966).

[53] G. D. Alkhazov, V. V. Anisovich, and P. E. Volkovyckii, *Diffractional Interaction of Hadrons with Nuclei at High Energies* (Nauka, Leningrad, 1991), p. 94.

[54] V. V. Burov and V. K. Lukyanov, Preprint JINR, R4-11098, 1977, Dubna; V. V. Burov, D. N. Kadrev, V. K. Lukyanov, and Yu. S. Pol', Phys. At. Nucl. **61**, 525 (1998).

[55] J. Friedrich and Th. Walcher, Eur. Phys. J. A **17**, 607 (2003).

[56] G. G. Simon, Ch. Schmitt, F. Borkowski, and V. H. Walther, Nucl. Phys. **A333**, 381 (1980).

[57] S. Galster, H. Klein, J. Moritz, K. H. Schmidt, D. Wegener, and J. Bleckwenn, Nucl. Phys. **B32**, 221 (1971).

[58] H. Chandra and G. Sauer, Phys. Rev. C **13**, 245 (1976).

[59] H. De Vries, C. W. De Jager, and C. De Vries, At. Data Nucl. Data Tables **36**, 495 (1987).

[60] I. Sick, Phys. Lett. **B116**, 212 (1982).

[61] J. D. Patterson and R. J. Peterson, Nucl. Phys. **A717**, 235 (2003).

[62] E. Friedman, A. Gal, and J. Mares, Nucl. Phys. **A579**, 518 (1994).

[63] D. Vautherin, Phys. Rev. C **7**, 296 (1973).

[64] Technical Proposal for the Design, Construction, Commisioning and Operation of the ELISe Setup, H. M. Simon, spokesperson (2005).

[65] J. S. McCarthy, I. Sick, and R. R. Whitney, Phys. Rev. C **15**, 1396 (1977).

[66] C. R. Ottermann *et al.*, Nucl. Phys. **A436**, 688 (1985).

[67] L. R. Suelzle, M. R. Yearian, and Hall Crannell, Phys. Rev. **162**, 992 (1967).

[68] G. C. Li, I. Sick, R. R. Whitney, and M. R. Yearian, Nucl. Phys. **A162**, 583 (1971).

[69] I. Sick, J. B. Bellicard, M. Bernheim, B. Frois, M. Huet, Ph. Leconte, J. Mougey, Phan Xuan-Ho, D. Royer, and S. Turck, Phys. Rev. Lett. **35**, 910 (1975).

[70] A. S. Litvinenko *et al.*, Yad. Fiz. **14**, 40 (1971) [Sov. J. Nucl. Phys. **14**, 23 (1972)]

[71] A. S. Litvinenko *et al.*, Nucl. Phys. **A182**, 265 (1972).

[72] T. H. Curtis, R. A. Eisenstein, D. W. Madsen, and C. K. Bockelman, Phys. Rev. **184**, 1162 (1969).

[73] J. W. Lightbody, Jr., S. Penner, S. P. Fivozinsky, P. L. Hallowell, and H. Crannell, Phys. Rev. C **14**, 952 (1976).

[74] J. Cavedon, J. B. Bellicard, B. Frois, D. Goutte, M. Huet, P. Leconte, X.-H. Phan, S. K. Platchkov, and I. Sick, Phys. Lett. **B118**, 311 (1982).

[75] H. Überall, *Electron Scattering from Complex Nuclei* (Academic Press, New York, 1971).

[76] M. Keim *et al.*, Nucl. Phys. **A586**, 219 (1995).

[77] D. Abbott *et al.*, Eur. Phys. J. A **7**, 421 (2000).

[78] A. Ozawa, T. Suzuki, and I. Tanihata, Nucl. Phys. **A693**, 32 (2001).

[79] W. J. Swiatecki, A. Trzcinska, and J. Jastrzebski, Phys. Rev. C **71**, 047301 (2005).